First-principles study of electronic transport in germanane and hexagonal boron nitride

Mohammad Mahdi Khatami [1,2,*] Maarten L. Van de Put,[2] and William G. Vandenberghe [2,†]

[1]*Faculty of Electrical and Computer Engineering, Tarbiat Modares University, P. O. Box 14115-194, Tehran 1411713116, Iran*

[2]*Department of Materials Science and Engineering, The University of Texas at Dallas, Richardson, Texas 75080, USA*

(Received 26 August 2021; revised 5 November 2021; accepted 30 November 2021; published 20 December 2021)

We present a detailed first-principles study on phonon-limited electronic transport in germanane and hexagonal boron nitride (h-BN). We find a high electron mobility of 2380 $cm^2\,V^{-1}\,s^{-1}$ and a low hole mobility of 60 $cm^2\,V^{-1}\,s^{-1}$ for germanane. For h-BN, we also find a respectable electron mobility of 118 $cm^2\,V^{-1}\,s^{-1}$ together with a high hole mobility of 444 $cm^2\,V^{-1}\,s^{-1}$. H-BN does not suffer from scattering associated with out-of-plane (flexural) acoustic (ZA) phonons due to its σ_h symmetry, but germanane does. Different cutoff wavelengths (λ_{cutoff}), ranging from 0.4 to 17.6 nm, are considered to simulate the possible effect of a supporting substrate on the ZA phonons for germanane. Increasing λ_{cutoff} results in a degradation of the mobility down to 1640 $cm^2\,V^{-1}\,s^{-1}$ for electrons and 1 $cm^2\,V^{-1}\,s^{-1}$ for holes assuming $\lambda_{cutoff} = 17.6$ nm. We also study transport in the presence of a homogeneous electric field E. A negative electron differential mobility is observed in germanane for $E > 10^4$ V cm^{-1} due to transfer to the higher effective-mass M valleys. Finally, the calculated mobilities are compared with those obtained for other two-dimensional (2D) materials, showing that germanane has the highest electron mobility, whereas holes in h-BN have the third highest mobility in our list of materials, outperformed only by WS_2 and WSe_2. This shows that germanane and h-BN can be considered for future nanoscaled electronic devices. Finally, the high germanane mobility shows that 2D materials can outperform bulk materials if the right material is found and if scattering with acoustic flexural phonons can be suppressed.

DOI: 10.1103/PhysRevB.104.235424

I. INTRODUCTION

Two-dimensional (2D) materials are considered possible channel materials for transistor applications thanks to their potential to allow better scaling than current electronic devices that suffer from deteriorated subthreshold slope, mobility degradation, drain-induced barrier lowering, and increased tunneling current through the gate oxide [1]. Over 1000 2D materials have been proposed so far, and many researchers are looking for the most suitable material to be used in future devices [2–4]. Generally, two properties of the channel material are key for complementary metal-oxide-semiconductor applications: (1) a good mobility to give high on-current and (2) an electronic bandgap >0.4 eV to ensure an acceptable I_{on}/I_{off} ratio ($>10^4$) [5].

Germanane, a hydrogen-terminated monolayer of bulk ⟨111⟩ germanium, has been investigated for electronic applications [6,7] both theoretically [8–12] and experimentally [13,14], demonstrating a sufficiently high bandgap in its chairlike configuration, the most stable morphology [10–12]. Moreover, germanane is based on Ge and H, two common elements currently used in the electronic industry, facilitating possible future integration in a technology. On the other side, hexagonal boron nitride (h-BN) has also been a popular material for future electronic devices, especially because of its high thermal conductivity [15,16] which can assist heat dissipation in very large-scale integrated devices. However, because of its large bandgap [17–21], it has been considered mostly as an insulator, and only a few groups [22–24] have investigated its electronic applications.

To assess the potential of germanane and h-BN for nano-electronic applications, a detailed study is required to calculate their carrier mobility and other transport properties. Such a study can be performed by solving the Boltzmann transport equation (BTE) and by using the electronic and vibrational properties of materials calculated from *ab initio* methods based on density functional theory (DFT) [25–33]. A careful investigation is crucial to ensure correct results, especially when dealing with the out-of-plane (flexural) acoustic (ZA) phonons [34–36]. Scattering with the ZA phonons, which have a parabolic dispersion relation, is often the most important scattering mechanism in 2D materials that do not exhibit horizontal mirror (σ_h) symmetry because of the Mermin-Wagner theorem [37–40]. However, several physical mechanisms, such as the clamping of these modes caused by the substrate [41,42] (and/or gate oxide), can significantly suppress the amplitude of these vibrations and thus the strength of the scattering process associated with the long wavelength ZA phonons. This influence can be considered through introducing a cutoff wavelength λ_{cutoff} and suppressing the ZA phonons whose wavelength is larger than λ_{cutoff} [40].

Bianco *et al.* [14] and Restrepo *et al.* [43] have investigated electron mobility in germanane and obtained a very high value of ∼18 200 $cm^2\,V^{-1}\,s^{-1}$. However, they did not explain how they dealt with the ZA phonons, and little detail was

*mm.khatami@modares.ac.ir

†william.vandenberghe@utdallas.edu

provided about the numerical implementation of their calculations, such as **k** and **q** (electron and phonon wave vectors) meshes used, two key factors in mobility calculations [28,44]. For h-BN, a theoretical estimation of the electron mobility of $487\,\mathrm{cm}^2\,\mathrm{V}^{-1}\,\mathrm{s}^{-1}$ was made by Bruzzone and Fiori [23] using the Takagi formula [45]. At best, this formula—and the simplification it entails—can give only a rough estimate of the mobility, but it can be quantitatively highly misleading. For example, Bruzzone and Fiori [23] only considered scattering with longitudinal acoustic (LA) phonons, assuming a constant deformation potential, ignoring the angular dependence of the electron-phonon matrix elements.

In this paper, we perform first-principles calculations of the electron and hole mobility in germanane, in its chairlike configuration, and h-BN. First, we determine the basic properties of each material (viz., atomic structure, electronic excitation spectrum, phonon dispersion, and electron-phonon matrix elements) using DFT in combination with density functional perturbation theory (DFPT). Then we calculate the strength of the electron-phonon interaction, highlighting the phonon branches that affect transport most significantly. Finally, the BTE is solved stochastically using a full-band Monte Carlo method [34] to calculate the low-field carrier mobility and drift velocity in the presence of a homogeneous external electric field. The possible role of the substrate in weakening the interaction of electrons with ZA phonons is simulated by considering different cutoff wavelengths for these flexural modes, as discussed in Ref. [40]. Finally, the calculated mobilities are compared with those obtained for other 2D semiconductors. This comparison shows that germanane and h-BN are promising candidates for future electronic applications.

II. COMPUTATIONAL METHODS

First-principles calculations were performed using the QUANTUM ESPRESSO (QE) DFT package [46,47] using optimized norm-conserving Vanderbilt pseudopotentials [48] and the Perdew-Burke-Ernzerhof (PBE) form generalized gradient approximation (GGA) [49]. A zone-centered Monkhorst-Pack [50] **k**-grid of $24 \times 24 \times 1$ was used with a maximum kinetic energy cutoff of 50 Ry for the plane-wave basis sets and 200 Ry for the charge density and potential. A vertical spacing of 2.5 nm was considered between periodically replicated monolayers to minimize the interaction between adjacent supercells. We note a small error will be present in our results because of periodic images [51]. Structural optimization was performed until the change in total energy was $<3 \times 10^{-5}$eV and the atomic forces were $<5 \times 10^{-4}\,\mathrm{eV\,\AA^{-1}}$.

The dynamic properties were determined using DFPT as implemented in the QE package using a uniform grid of $12 \times 12 \times 1$ for phonon wave vectors **q**. The electron-phonon interaction matrix element for the transition of an electron with an initial state ψ_i with a wave vector $\mathbf{k}_i = \mathbf{k}$ to a final state ψ_j with a wave vector of $\mathbf{k}_j = \mathbf{k} + \mathbf{q}$ was determined by

$$g^{ijv}_{\mathbf{kq}} = \sqrt{\frac{\hbar}{2M_{\mathrm{cell}}\omega_{\mathbf{q},v}}}\langle\psi_{j,\mathbf{k}+\mathbf{q}}|\partial V^{\mathrm{SCF}}_{\mathbf{q},v}|\psi_{i,\mathbf{k}}\rangle, \tag{1}$$

in which $\hbar$ and M_{cell} are the reduced Plank's constant and the mass of the unit cell. Here, $\partial V^{\mathrm{SCF}}_{\mathbf{q},v}$ is the change of the self-consistent potential due to a phonon of branch v, wave vector **q**, and frequency $\omega_{\mathbf{q},v}$.

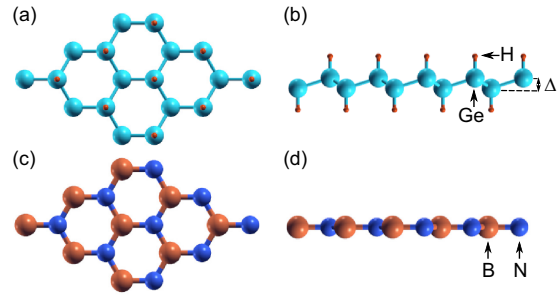

FIG. 1. Top and side views of (a) and (b) germanane and (c) and (d) h-BN structures.

To obtain numerically accurate results, the material properties must be tabulated and interpolated using a very fine mesh in the Brillouin zone (in this paper, $150 \times 150 \times 1$). The electronic band structure was calculated directly on this fine mesh, but computational costs prevent us from using such a mesh when calculating phonon energies and electron-phonon interaction matrix elements. Therefore, these were interpolated on a coarser grid of $50 \times 50 \times 1$ using maximally localized Wannier functions [52,53], as implemented in the EPW computer program [54]. Then a linear interpolation was used to obtain phonon energies and electron-phonon matrix elements on the final $150 \times 150 \times 1$ grid.

The scattering rates for each phonon branch were calculated using Fermi's golden rule:

$$\frac{1}{\tau^{v}_{i,\mathbf{k}}} = \frac{2\pi}{\hbar}\sum_{j,\mathbf{q}}\left|g^{ijv}_{\mathbf{kq}}\right|^2[N_{\mathbf{q},v}\delta(E_{j,\mathbf{k}+\mathbf{q}} - \hbar\omega_{\mathbf{q},v} - E_{i,\mathbf{k}}) + (N_{\mathbf{q},v}+1)\delta(E_{j,\mathbf{k}-\mathbf{q}} + \hbar\omega_{\mathbf{q},v} - E_{i,\mathbf{k}})], \tag{2}$$

where the first and second terms on the right side correspond to absorption and emission processes. Here, $N_{\mathbf{q}}$, v is the Bose-Einstein phonon occupation:

$$N_{v,\mathbf{q}} = \left[\exp\left(\frac{\hbar\omega_{\mathbf{q},v}}{k_B T}\right) - 1\right]^{-1}, \tag{3}$$

where k_B and T denote the Boltzmann constant and the lattice temperature.

Having obtained the scattering rates, electronic transport was studied with a full-band Monte Carlo method [34]. This method monitors the trajectory of 300 carriers in time steps of 0.1 fs for a total duration of 100 ps. To minimize stochastic noise, the zero-field intrinsic mobility was obtained from the diffusion constant via the Einstein relation. The mobility can also be extracted from the velocity-field characteristics, albeit with a larger stochastic noise [55]. The transient time [55] was estimated as 20 ps in both materials under consideration, and all mobilities and velocities were calculated by averaging over the last 80 ps of the calculations as the steady state.

III. RESULTS AND DISCUSSIONS

A. Material parameters

Figure 1 shows the relaxed honeycomb structure of germanane and h-BN. Whereas h-BN exhibits a planar structure,

TABLE I. Structural and electronic properties of germanane and h-BN.

Symbol	Description	Germanane	h-BN	Unit
a	Lattice constant	4.068	2.51	Å
Δ	Buckling height	0.736	0	Å
m_e	Electron effective mass	0.064	$(K \rightarrow \Gamma)$: 0.83 $(K \rightarrow M)$: 1.15	m_0
m_h	Hole effective mass	LH[a]: 0.064 HH[b]: 0.56	$(K \rightarrow \Gamma)$: 0.57 $(K \rightarrow M)$: 0.77	m_0
E_G	Bandgap	1.044	4.68	eV
b		1.6×10^{-7}	4.2×10^{-7}	m^2/s
υ_{TA}	Sound velocity of the TA mode	3.2×10^3	1.22×10^4	m/s
υ_{LA}	Sound velocity of the TA mode	5.1×10^3	1.91×10^4	m/s

[a]Light hole.
[b]Heavy hole.

germanane is buckled, thus breaking the σ_h symmetry found in planar honeycomb structures like graphene or h-BN. Structural parameters and basic electronic characteristics of germanane and h-BN are listed in Table I. The lattice constants we have obtained are 4.068 Å for germanane (in agreement with [8,9,11]) and 2.51 Å for h-BN (in agreement with [18,20,23,56]).

Figure 2(a) shows the calculated electronic band structures of germanane and the associated projected density of states (PDOS). Germanane has a direct bandgap of 1.04 eV at Γ. This is accompanied by a very small effective mass of electrons (m_e) in germanane ($0.064\,m_0$), which may result in a high electron mobility. Both the conduction and the valence bands of germanane are isotropic around their extrema at Γ, providing isotropic effective masses for electrons and holes. While the conduction band minimum of germanane consists of only one band, the valence band maximum is degenerate, consisting of light and heavy hole bands, both taking part in electronic transport. Other local conduction band minima, with an energy 0.92 eV higher than the minimum at Γ, can be observed at the M symmetry points. Thus, electrons are expected to populate the Γ valley at low fields but may scatter to the M valleys at higher fields.

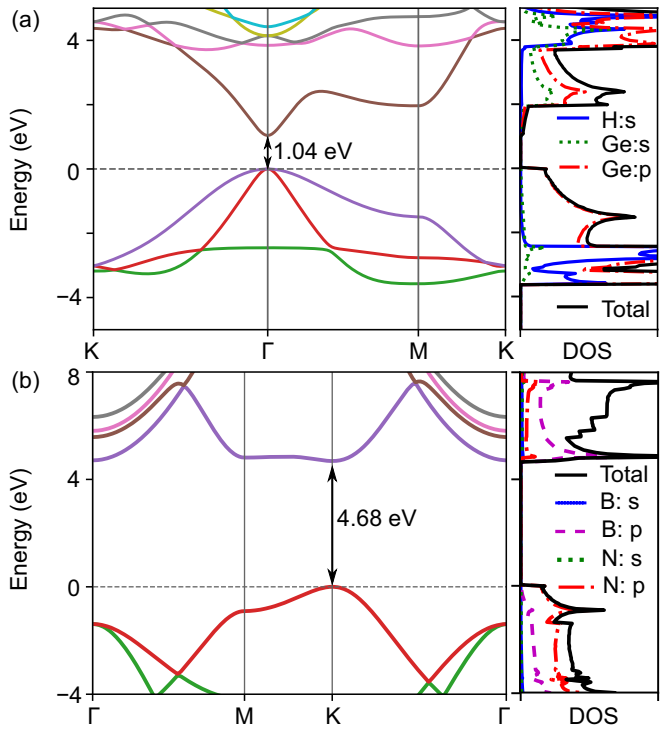

FIG. 2. Electronic band structure of (a) germanane and (b) h-BN along high symmetry lines of the first Brillouin zone. The right-hand sides of (a) and (b) represent the associated projected density of states.

Figure 2(b) shows the band structure of h-BN and its PDOS, exhibiting a large direct bandgap of 4.68 eV at the K point. This is larger than the bandgaps of several wide-gap materials, such as graphane monolayer (3.466 eV [57]), graphene fluoride monolayer (3.208 eV [57]), bulk SiC (3.205 [58]), or bulk GaN (3.4 eV), and lower than the bandgap of diamond (5.47 eV [59]). The conduction band of h-BN exhibits local minima located at the M symmetry points, only 25 meV ($\sim k_B T$) higher than the minima at the K points. Thus, at room temperature, electrons are expected to populate both the M and K valleys and even the path between them. Moreover, the energy of the local minimum at Γ is only 127 meV above the minima at K. Therefore, also the Γ valley is likely to play a role in electron transport at large external electric fields.

The PDOS inset of Fig. 2(a) shows that the conduction band minimum of germanane is made up of p and s orbitals of Ge atoms, while the valence band maximum is mostly formed by p orbitals of Ge atoms. On the other side, Fig. 2(b) shows that the conduction band minima of h-BN originate mostly from p orbitals of B atoms, while its valence band maxima are constituted by the p orbitals of the N atoms.

It is worth noting that the only experimental data on bandgaps of germanane and h-BN are the optical bandgaps, 1.59 eV [14] in germanane and 5.62 eV in h-BN [17]. The lower bandgaps calculated in this paper are likely the result of the well-known underestimation of DFT calculations with the GGA-PBE exchange-correlation functional.

Figure 3 shows the calculated phonon dispersion and the corresponding PDOS for germanane and h-BN. Germanane exhibits 12 branches, originating from the four atoms (2Ge + 2H) forming its unit cell. In contrast, the h-BN unit cell consists of two atoms (B + N), resulting in six phonon branches. In both materials, as expected for a 2D material [40], a

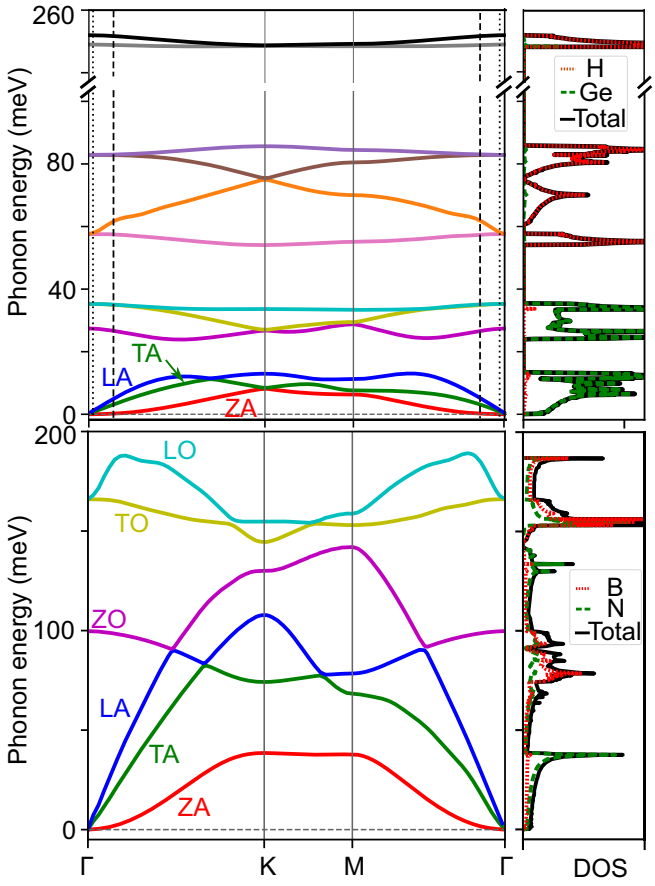

FIG. 3. Phonon dispersion of (a) germanane and (b) h-BN along high symmetry lines of the first Brillouin zone. The right-hand sides of (a) and (b) represent the associated projected density of states. The dashed and dotted lines in phonon dispersion of germanane indicate the wave vectors associated with cutoff wavelengths of 4.2 and 17.6 nm, respectively.

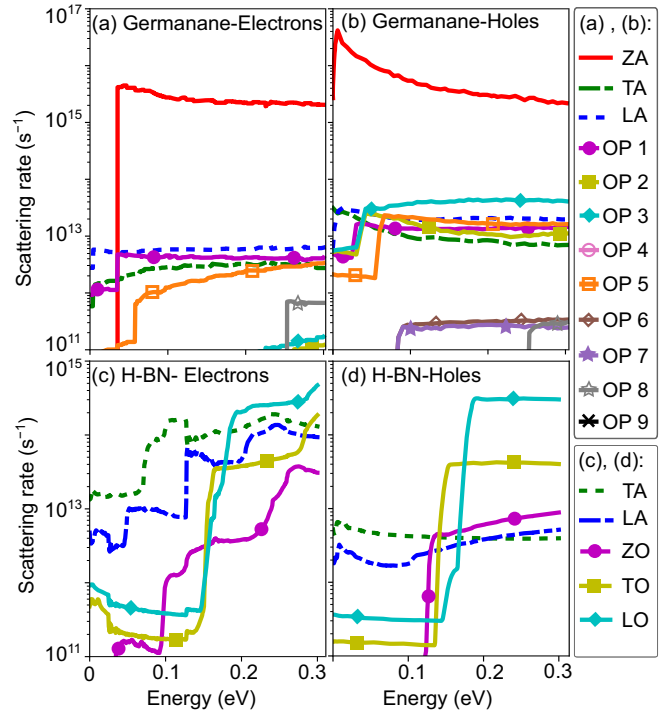

FIG. 4. Calculated scattering rates for (a) and (c) electrons and (b) and (d) holes in (a) and (b) germanane and (c) and (d) h-BN at room temperature ($T = 300$ K). A cutoff wavelength of 17.6 nm is used to simulate the possible effect of a supporting substrate on the ZA phonons.

quadratic dispersion relation ($\omega_{\mathbf{q},v} = bq^2$) is observed for the ZA phonons around Γ. The other two acoustic branches (TA and LA) have a linear dispersion relation close to Γ. The values of b and sound velocities associated with the TA and LA modes are given in Table I.

The PDOS shows that the acoustic modes in germanane originate mostly from the motion of the Ge atoms because of their heavier atomic mass (72.63 u) than the H atoms (1.008 u). The Ge atoms are also responsible for the three lowest energy optical branches. The remaining optical phonon branches, including the two high-energy phonons (∼250 meV), are mostly associated with the vibration of the H terminating atoms. In h-BN, nitrogen is the heaviest ion (14.007 u compared with the B atoms with an atomic mass of 10.81 u) and dominate the acoustic modes.

B. Scattering rates

Three different cutoff wavelengths λ_{cutoff} are used in this paper to simulate the possible effect of a supporting substrate on the long-wavelength dispersion of the ZA phonons of germanane. A cutoff wavelength of $\lambda_{\text{cutoff}} = 0.6$ nm is considered the first case. This wavelength is associated with the first Brillouin zone edge [$q = 4\pi/(3a)$], and thus, all the ZA phonons will be suppressed completely. The second λ_{cutoff} is determined following the results provided in Refs. [41,42], where the effect of a supporting substrate on the ZA phonons of graphene is studied. Based on these works, the onset of change in the dispersion relation of the ZA phonons on different substrates ranges from 0.3 to 1 Å^{-1}. Considering the worst case, the cutoff wave vector is $q_{\text{cutoff}} = 0.3$Å$^{-1} \sim 0.1q_0$, in which $q_0 = 4\pi/(\sqrt{3}a)$, and a is the lattice constant. In this paper, the first q point in DFPT calculations after Γ, $q = q_0/12$, will be used to simulate this case which is associated with $\lambda_{\text{cutoff}} = 4.2$ nm. A larger cutoff wavelength $\lambda_{\text{cutoff}} = 17.6$ nm is also considered the last case if none of the first two scenarios came true.

The calculated scattering rates for electrons and holes in germanane and h-BN are shown in Fig. 4 (see the Supplemental Material for the electron-phonon interaction matrix elements [60]). The scattering rates of germanane are calculated under the cutoff wavelength of 17.6 nm. The σ_h symmetry of h-BN prohibits a first-order intraband interaction between ZA phonons and electrons/holes. Therefore, in h-BN, ZA phonons will have a negligible effect on the scattering mechanisms, and no cutoff for the ZA phonons was considered for this material.

As expected for a 2D material without σ_h symmetry, interactions with the ZA phonons result in the highest scattering rates in germanane. However, assuming $\lambda_{\text{cutoff}} = 17.6$ nm, the scattering rates of the ZA phonons become negligible for electrons whose energy is lower than a cutoff energy (E_{cutoff})

TABLE II. Calculated mobilities of electrons and holes for germanane at room temperature and for three different cutoff wave vectors (q_{cutoff}) as $3^{-1/2}\ q_0$, $12^{-1}\ q_0$, and $50^{-1}\ q_0$ in which $q_0 = 4\pi\ (3^{1/2}\ a)^{-1}$. λ_{cutoff} represents cutoff wavelength associated with each q_{cutoff}. Mobilities of electrons and holes in graphane ($a = 2.535$ Å) [57] and silicane ($a = 3.887$ Å) [66] are also shown for comparison.

	Graphane			Silicane			Germanane		
		Mobility ($\text{cm}^2\ \text{V}^{-1}\ \text{s}^{-1}$)			Mobility ($\text{cm}^2\ \text{V}^{-1}\ \text{s}^{-1}$)			Mobility ($\text{cm}^2\ \text{V}^{-1}\ \text{s}^{-1}$)	
q_{cutoff}	λ_{cutoff} (nm)	μ_e	μ_h	λ_{cutoff} (nm)	μ_e	μ_h	λ_{cutoff} (nm)	μ_e	μ_h
$3^{-1/2}\ q_0$	0.4	278	391	0.58	53	109	0.6	2380	60
$12^{-1}\ q_0$	2.6	233	389	4	24	101	4.2	2380	55
$50^{-1}\ q_0$	11	28	41	16	5	10	17.6	1640	1

of 27.5 meV. The difference between E_{cutoff} of electrons and holes can be explained through the scattering mechanism of the ZA phonons. Due to the very low energies of the long-wavelength ZA phonons, their induced scatterings can be assumed as elastic. Thus, only phonons with a wave vector of $q < 2k$ are allowed to play a role in the scattering process. This means that, under a cutoff wave vector of q_{cutoff}, the electrons or holes with $k < q_{\text{cutoff}}/2$ will not be affected by the ZA phonons. This wave vector translates to a cutoff energy which can be calculated from $E_{\text{cutoff}} = \hbar^2 k^2/2m^*$. Electrons of germanane have much smaller effective mass ($0.064\,m_0$) than holes ($0.56\,m_0$ for heavy holes which have a higher probability of occupation due to their lower energy than light holes). This results in higher E_{cutoff} for electrons than holes.

The second highest rates in germanane are found for scattering with the TA and LA branches because of their lower energy than the optical branches, resulting in higher phonon occupation numbers [Eq. (3)]. For h-BN, the highest scattering rates are associated with the TA and LA branches.

A steplike increase can be observed in scattering rates of optical phonons in germanane and h-BN at the corresponding phonon energies (e.g., a steplike increase at $E \sim 27.5$ meV in scattering rates of OP1 in germanane). This is attributed to the emission process when the carriers have enough energy to emit the corresponding phonons. The significant scattering rates of the LO mode in h-BN can be attributed to the Frölich interaction [61,62] because of its polar nature.

Several steplike increases and distortions can also be observed in scattering rates of electrons in h-BN. The reason behind the distortions is the very small energy difference between the K and M valleys ($\sim k_B T$), providing various low-energy states where the electrons can scatter to. Additionally, the steplike increases can be related to the scattering of electrons between the K, M, and Γ valleys.

Since h-BN is polar and a 2D material, there is a $1/q$ divergence of the matrix elements associated with the LO mode [63], where a singularity is avoided by our interpolation scheme. However, the error on mobility, associated with the interpolation or by the Fröhlich interaction between periodic images [64,65], will be minimal because of the very high energy of the LO phonons resulting in very small phonon occupation numbers.

C. Electron and hole mobility

In Table II, we list the electron and hole mobility that we have obtained for germanane using different cutoff wavelengths for the flexural phonons. We also show for comparison the carrier mobilities in graphane (hydrogenated graphene) [57] and silicane (hydrogenated silicene) [66] taken from our previous work using similar ZA-phonon cutoff wave vectors.

The highest electron ($2380\,\text{cm}^2\ \text{V}^{-1}\ \text{s}^{-1}$) and hole mobility ($60\,\text{cm}^2\ \text{V}^{-1}\ \text{s}^{-1}$) in germanane is obtained with complete suppression of the ZA phonons ($\lambda_{\text{cutoff}} = 0.6$ nm). The calculated hole mobility is very close to the experimentally measured value of $70\,\text{cm}^2\ \text{V}^{-1}\ \text{s}^{-1}$ [7] and indicates that a strong suppression of ZA phonons is experimentally possible in germanane. Choosing a higher $\lambda_{\text{cutoff}} = 4.2$ nm, only ZA phonons with $q > 2\pi\,\lambda_{\text{cutoff}}^{-1}$ are involved in the scattering process. Although this λ_{cutoff} decreases the hole mobility, no considerable change is observed in the electron mobility. Obviously, increasing the cutoff wavelength to 17.6 nm causes ZA phonons with a small wave vector to participate in the scattering events, resulting in a lower electron mobility of $1640\,\text{cm}^2\ \text{V}^{-1}\ \text{s}^{-1}$ and a very low hole mobility of $1\,\text{cm}^2\ \text{V}^{-1}\ \text{s}^{-1}$.

To better understand the reason behind these behaviors, a closer look into the scattering mechanisms would be helpful. Average energy of electrons (holes) at room temperature can be estimated as $\sim k_B T$, associated with a wave vector of $\sqrt{2mk_BT}/\hbar$. On the other hand, the scattering process due to the long-wavelength ZA phonons can be assumed as elastic. Thus, important phonons in the scattering process are the ones whose wave vectors are $< 2 \times \sqrt{2mk_BT}/\hbar$. This is associated with a wavelength of ~15.1 nm for electrons and ~5 nm for holes in germanane, and no significant reduction is expected in the mobility without including the ZA phonons whose wavelength is larger than the corresponding λ. Here, $\lambda_{\text{cutoff}} = 4.2$ nm is much lower than the critical wavelength of 15.1 nm for electrons. Thus, the electron mobility remains almost the same as $\lambda_{\text{cutoff}} = 0.6$ nm. In the case of holes, $\lambda_{\text{cutoff}} = 4.2$ nm is very close to the critical wavelength of 5 nm. However, a few holes whose energy is higher than the average energy ($k_B T$) will be affected by the ZA phonons, resulting in a small reduction (8.3%) in their mobility. Here, $\lambda_{\text{cutoff}} = 17.6$ nm allows some of the important ZA phonons to play role in scattering of electrons, resulting in ~31% decrease in the electron mobility. More important ZA phonons will be allowed in scatterings of holes under $\lambda_{\text{cutoff}} = 17.6$ nm, resulting in a significant degradation of the hole mobility.

In the case of h-BN, its σ_h symmetry prohibits the ZA phonons from playing a significant role, yielding relatively high mobilities of $118\,\text{cm}^2\ \text{V}^{-1}\ \text{s}^{-1}$ for electrons and

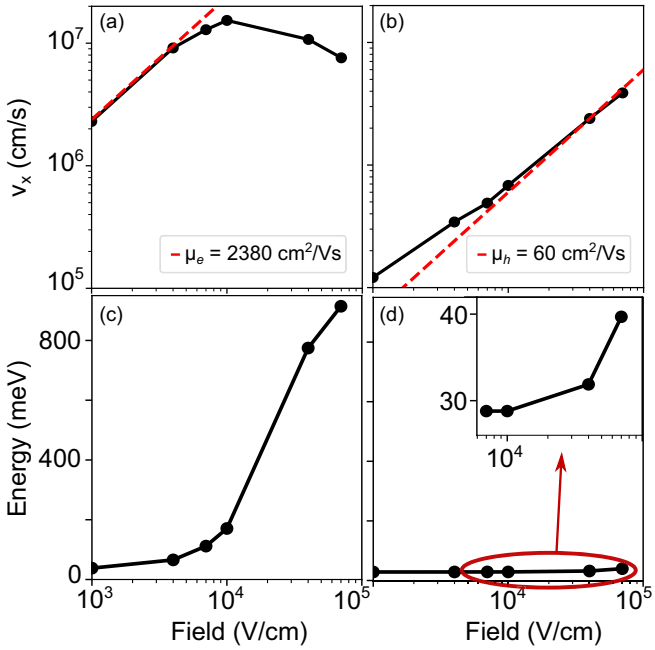

FIG. 5. The effect of an applied electric field along the armchair x direction on (a) and (b) velocity and (c) and (d) average energy of (a) and (c) electrons and (b) and (d) holes in germanane at room temperature ($T = 300$ K). The dashed line indicates the mobility calculated from the diffusion constant.

444 cm^2 V^{-1} s^{-1} for holes. The lower electron mobility (than hole) is the simple consequence of the many possible intervalley scattering paths among the three low-energy valleys

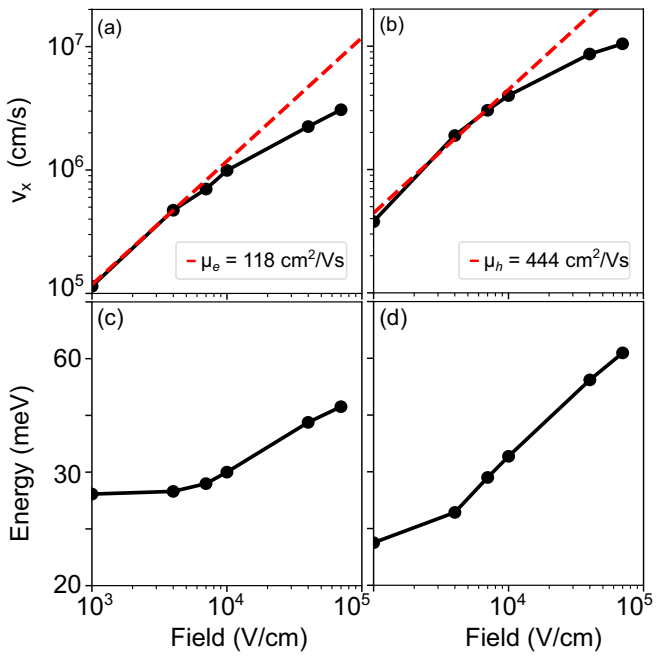

FIG. 6. The effect of an applied electric field along the armchair x direction on (a) and (b) velocity and (c) and (d) average energy of (a) and (c) electrons and (b) and (d) holes in h-BN at room temperature ($T = 300$ K). The dashed line indicates the mobility calculated from the diffusion constant.

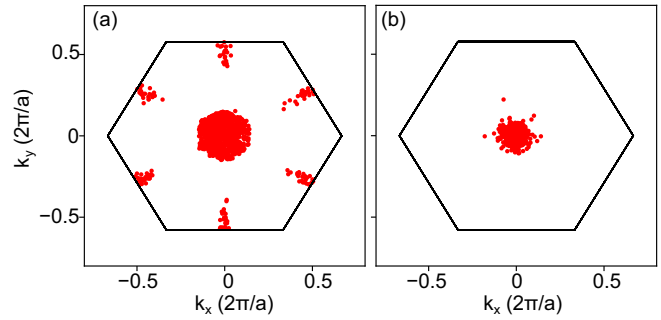

FIG. 7. Distribution of (a) electrons and (b) holes in the first Brillouin zone of germanane at an electric field of $E = 7 \times 10^4$ V cm^{-1} along the armchair x direction at room temperature ($T = 300$ K).

(K, M, and Γ). The only experimental information about hole transport in h-BN is provided by Bilal *et al.* [24], who report a hole mobility ranging from 225 to 280 cm^2 V^{-1} s^{-1} for h-BN on different substrates. Their lower mobility may be the result of nonidealities such as N vacancies, as mentioned by Bilal *et al.* [24].

D. Velocity field characteristics

The effect of an applied electric field along the armchair (x) direction on the velocity and average energy of electrons and holes in germanane and h-BN is shown in Figs. 5 and 6, respectively. The ZA phonons in germanane are assumed to be suppressed completely using the cutoff wavelength of 0.6 nm. The slope of υ-E at low fields is very close to the mobility calculated at zero electric field. Increasing the electric field results in a reduction of the differential mobility that, in the case of electrons in germanane, becomes negative for $E > 10^4$ V cm^{-1}.

To better understand the reason behind the influence of the increasing electric field, the distribution of electrons and holes in reciprocal space at $E = 7 \times 10^4$ V cm^{-1} is shown in Fig. 7 for germanane and Fig. 8 for h-BN. At low electric fields, in germanane, electrons are confined to the conduction band minimum at Γ. Increasing E will increase the average energy of electrons up to 0.92 eV at $E = 7 \times 10^4$ V cm^{-1}. As a result, some electrons will gain enough energy to overcome the difference between the Γ and M valleys (0.92 eV). The

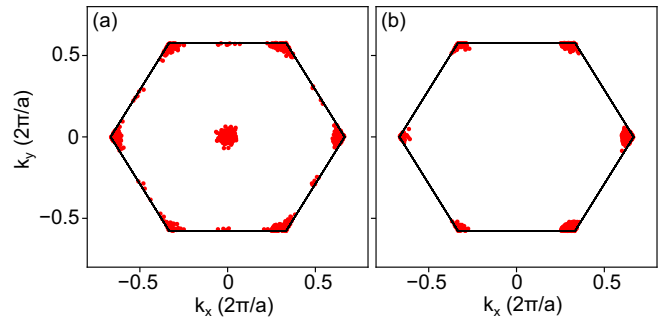

FIG. 8. Distribution of (a) electrons and (b) holes in the first Brillouin zone of h-BN at an electric field of $E = 7 \times 10^4$ V cm^{-1} along the armchair x direction at room temperature ($T = 300$ K).

scattering of electrons to the M valleys with higher effective mass ($m^{\mathrm{M}\to\Gamma}_{e,\mathrm{germanane}} = 3.6m_0$, $m^{\mathrm{M}\to\Gamma}_{e,\mathrm{germanane}} = 0.12m_0$) than the Γ valley ($m^{\Gamma}_{e,\mathrm{germanane}} = 0.064m_0$) results in a negative slope of υ-E. This case is like the negative differential mobility of electrons which takes place in GaAs when electrons transition from the Γ valley to the L valleys (with higher effective mass) as a result of an external electric field [67–69].

No intervalley scattering is observed in the case of holes in germanane and h-BN, and the differential mobility remains positive up to the highest value of the electric field that we have considered. In the case of electrons in h-BN, electrons occupy the K and M valleys at low electric fields because of the small energy difference between the minima of these valleys. Increasing the electric field results in scattering of electrons to the Γ valley with effective mass of $m^{\Gamma}_{e,\text{h-BN}} = 0.98m_0$. This is very close to the effective mass of the electrons in the K valleys ($m^{\mathrm{K}\to\Gamma}_{e,\text{h-BN}} = 0.83m_0$, $m^{\mathrm{K}\to\mathrm{M}}_{e,\text{h-BN}} = 1.15m_0$) and does not result in a negative slope of υ-E up to the applied electric fields.

IV. MATERIALS COMPARISON

In Table III, we compare the calculated mobilities of electrons and holes with those of other 2D semiconductors which have been previously studied with similar methods. This is to avoid the discrepancies in carrier mobilities observed when using different methods [34]. The ZA phonons have been suppressed completely in materials that lack σ_h symmetry, i.e., graphane, silicane, germanane, and graphene fluoride.

The highest electron mobility can be seen in germanane, exceeding the next highest value by more than a factor of 5, as reported for graphene fluoride. Although electrons in h-BN only exhibit the seventh highest mobility, h-BN still exhibits a good mobility when comparing with other popular transition metal dichalcogenides, such as MoS_2, $MoSe_2$, and WSe_2. For the hole mobility, h-BN exhibits a very good mobility and is only outperformed by WS_2 and WSe_2. On the other side, germanane has moderately low hole mobility compared to the materials in the comparison list.

Regarding the results we have obtained for germanane, the electron mobility is particularly remarkable when factoring in the theoretical considerations presented by Cheng *et al.* [70], who revealed fundamental disadvantages in 2D materials in terms of mobility. Before this study, the possibility of surpassing the electron mobility of bulk silicon ($1450\,\mathrm{cm^2\,V^{-1}\,s^{-1}}$ [74]) was certainly not expected. There are two main factors behind the high germanane electron mobility. First, the effective mass of electrons in germanane ($0.064\,m_0$) is much smaller than in bulk silicon (with transverse and longitudinal effective masses of $m_t = 0.19\,m_0$ and $m_l = 0.92m_0$, respectively [74]). Second, the sound velocity of the LA phonons in germanane ($\upsilon_{\mathrm{LA}} = 5.1 \times 10^3\,\mathrm{m\,s^{-1}}$), the process that yields the strongest scattering mechanism, is very close to the sound velocities of the TA phonons in bulk silicon ($\upsilon_{\mathrm{TA}} = 4.7 \times 10^3\,\mathrm{m\,s^{-1}}$), which are responsible for the highest scattering rates in bulk silicon [75].

One minor caveat regarding the high value of $2380\,\mathrm{cm^2\,V^{-1}\,s^{-1}}$ that we have obtained for the electron mobility in germanane is that we have assumed that the substrate causes a very strong suppression of the long-wavelength ZA phonons. However, even at $\lambda_{\mathrm{cutoff}} = 17.6\,\mathrm{nm}$, we obtained a mobility of $1640\,\mathrm{cm^2\,V^{-1}\,s^{-1}}$, indicating that, even with a relaxed cutoff, the ZA phonons still have a relatively minor impact on the scattering of electrons at the conduction band minimum, as illustrated in Fig. 4(a). Thus, the electrons in germanane are only affected by two (LA and TA) modes compared with silicon bulk with three (LA and 2TA) acoustic modes, also favoring germanane electron mobility. It is worth noting that this simple model for considering the substate effect on the ZA phonons might be reachable, according to the very similar hole mobility calculated in this paper ($60\,\mathrm{cm^2\,V^{-1}\,s^{-1}}$) and the experimentally measured value of $70\,\mathrm{cm^2\,V^{-1}\,s^{-1}}$ [7].

TABLE III. Comparison of the calculated intrinsic mobilities of electrons and holes in germanane and h-BN with other 2D semiconductors. The ZA phonons are completely suppressed in 2D materials without a σ_h symmetry, i.e., germanane, graphane, graphene fluoride, and silicane.

	Mobility ($\mathrm{cm^2\,V^{-1}\,s^{-1}}$)		
Material	μ_e	μ_h	Reference
Germanane	2 380	60	This paper
H-BN	118	444	This paper
Graphane	278	391	[57]
Graphene fluoride	460	105	[57]
Silicane	53	109	[66]
As	70	–	[70]
Bi	233	–	[70]
GaS	6.9	0.3	[70,71]
GaSe	39	0.4	[70,71]
GaTe	20	3.6	[70,71]
HfS_2	0.8	–	[70]
$HfSe_2$	2	–	[70]
InS	10	0.2	[70,71]
InSe	110	–	[72]
	18	0.3	[70,71]
InTe	29	0.6	[70,71]
MoS_2	130	270	[63,73]
	184	129	[70,71]
$MoSe_2$	25	90	[73]
	92	138	[70,71]
$MoTe_2$	43	43	[70,71]
$PdSe_2$	92	–	[70]
Phosphorene	10[a] (3)[b]	21[a] (19)[b]	[34]
PtS_2	29	–	[70]
$PtSe_2$	47	–	[70]
$PtTe_2$	35	–	[70]
Sb	81	–	[70]
SnS_2	5.7	–	[70]
$SnSe_2$	8.1	–	[70]
WS_2	320	540	[73]
	260	2182	[70,71]
WSe_2	30	270	[73]
	58	524	[70,71]
ZrS_2	0.8	–	[70]
$ZrSe_2$	1.4	–	[70]

[a]Zigzag
[b]Armchair

V. CONCLUSIONS

We have presented the results of a detailed *ab initio* study on electron and hole transport in germanane and h-BN monolayers. We first determined their basic electronic and vibrational properties using DFT in combination with DFPT. Germanane exhibited a direct bandgap of 1.04 eV at Γ, while h-BN had a wide direct bandgap of 4.68 eV at the *K* point.

The calculated carrier-phonon scattering rates emphasize the significant role of the ZA phonons in germanane, a material which lacks horizontal mirror (σ_h) symmetry. The effect of a possible supporting substrate on the ZA mode of germanane was simulated using different cutoff wavelengths λ_{cutoff} of 0.6, 4.2, and 17.6 nm. The highest mobility has been obtained for $\lambda_{\text{cutoff}} = 0.6\,\text{nm}$, $2380\,\text{cm}^2\,\text{V}^{-1}\,\text{s}^{-1}$ for electrons and $60\,\text{cm}^2\,\text{V}^{-1}\,\text{s}^{-1}$ for holes. The hole mobility was found to be only $55\,\text{cm}^2\,\text{V}^{-1}\,\text{s}^{-1}$ at $\lambda_{\text{cutoff}} = 4.2\,\text{nm}$, while the mobility of electrons was unaffected at the 4.2 nm cutoff. Further increasing λ_{cutoff} to 17.6 nm decreases hole mobility to $1\,\text{cm}^2\,\text{V}^{-1}\,\text{s}^{-1}$ and the electron mobility to $1640\,\text{cm}^2\,\text{V}^{-1}\,\text{s}^{-1}$. We have found that h-BN is not affected by ZA-phonon scattering, thanks to its σ_h symmetry, with calculated mobilities of $118\,\text{cm}^2\,\text{V}^{-1}\,\text{s}^{-1}$ for electrons and $444\,\text{cm}^2\,\text{V}^{-1}\,\text{s}^{-1}$ for holes.

We have also compared the calculated values of the mobility with those predicted for other 2D semiconductors to assess their competitiveness for application in future electronic devices. Here, h-BN has been shown to have a very high hole mobility, outperformed only by WS_2 and WSe_2. Finally and remarkably, the highest electron mobility was obtained for germanane ($2380\,\text{cm}^2\,\text{V}^{-1}\,\text{s}^{-1}$), a value that also surpasses the electron mobility in intrinsic bulk silicon. Ultimately, in this paper, we show that 2D materials can exhibit a high carrier mobility if the right material can be found, and in non-mirror-symmetric materials, flexural acoustic modes can be sufficiently damped by the supporting substrate.

ACKNOWLEDGMENT

The authors would like to acknowledge Professor Massimo V. Fischetti for having critically read this paper and for fruitful discussions.

The authors declare no conflicts of interest.

[1] M. V. Fischetti, B. Fu, and W. G. Vandenberghe, Theoretical study of the gate leakage current in sub-10-nm field-effect transistors, IEEE Trans. Electron Devices **60**, 3862 (2013).

[2] S. Kang, D. Lee, J. Kim, A. Capasso, H. S. Kang, J.-W. Park, C.-H. Lee, and G.-H. Lee, 2D semiconducting materials for electronic and optoelectronic applications: potential and challenge, 2D Mater. **7**, 022003 (2020).

[3] S. Haastrup, M. Strange, M. Pandey, T. Deilmann, P. S. Schmidt, N. F. Hinsche, M. N. Gjerding, D. Torelli, P. M. Larsen, A. C. Riis-Jensen, J. Gath, K. W. Jacobsen, J. Jørgen Mortensen, T. Olsen, and K. S. Thygesen, The computational 2D materials database: high-throughput modeling and discovery of atomically thin crystals, 2D Mater. **5**, 042002 (2018).

[4] M. Ashton, J. Paul, S. B. Sinnott, and R. G. Hennig, Topology-Scaling Identification of Layered Solids and Stable Exfoliated 2D Materials, Phys. Rev. Lett. **118**, 106101 (2017).

[5] B. Hoefflinger, ITRS: the international technology roadmap for semiconductors, in *Chips 2020: A Guide to the Future of Nanoelectronics*, edited by B. Hoefflinger (Semiconductor Industry Association, Washington, DC, 2011), pp. 161–174.

[6] M. Brahma, M. Bescond, D. Logoteta, R. K. Ghosh, and S. Mahapatra, Germanane MOSFET for subdeca nanometer high-performance technology nodes, IEEE Trans. Electron Devices **65**, 1198 (2018).

[7] B. N. Madhushankar, A. Kaverzin, T. Giousis, G. Potsi, D. Gournis, P. Rudolf, G. R. Blake, C. H. van der Wal, and B. J. van Wees, Electronic properties of germanane field-effect transistors, 2D Mater. **4**, 021009 (2017).

[8] V. Zólyomi, J. R. Wallbank, and V. I. Fal'ko, Silicane and germanane: tight-binding and first-principles studies, 2D Mater. **1**, 011005 (2014).

[9] K. L. Low, W. Huang, Y.-C. Yeo, and G. Liang, Ballistic transport performance of silicane and germanane transistors, IEEE Trans. Electron Devices **61**, 1590 (2014).

[10] R. K. Ghosh, M. Brahma, and S. Mahapatra, Germanane: a low effective mass and high bandgap 2-D channel material for future FETs, IEEE Trans. Electron Devices **61**, 2309 (2014).

[11] L. C. Lew Yan Voon, E. Sandberg, R. S. Aga, and A. A. Farajian, Hydrogen compounds of group-IV nanosheets, Appl. Phys. Lett. **97**, 163114 (2010).

[12] M. Houssa, E. Scalise, K. Sankaran, G. Pourtois, V. V. Afanas'ev, and A. Stesmans, Electronic properties of hydrogenated silicene and germanene, Appl. Phys. Lett. **98**, 223107 (2011).

[13] W. Amamou, P. M. Odenthal, E. J. Bushong, D. J. O'Hara, Y. Kelly Luo, J. van Baren, I. Pinchuk, Y. Wu, A. S. Ahmed, J. Katoch, M. W. Bockrath, H. W. K. Tom, J. E. Goldberger, and R. K. Kawakami, Large area epitaxial germanane for electronic devices, 2D Mater. **2**, 035012 (2015).

[14] E. Bianco, S. Butler, S. Jiang, O. D. Restrepo, W. Windl, and J. E. Goldberger, Stability and exfoliation of germanane: a germanium graphane analogue, ACS Nano **7**, 4414 (2013).

[15] Q. Cai, D. Scullion, W. Gan, A. Falin, S. Zhang, K. Watanabe, T. Taniguchi, Y. Chen, E. J. G. Santos, and L. H. Li, High thermal conductivity of high-quality monolayer boron nitride and its thermal expansion, Sci. Adv. **5**, eaav0129 (2019).

[16] X. Wu and Q. Han, Thermal conductivity of monolayer hexagonal boron nitride: from defective to amorphous, Comput. Mater. Sci. **184**, 109938 (2020).

[17] Y. Ji, B. Calderon, Y. Han, P. Cueva, N. R. Jungwirth, H. A. Alsalman, J. Hwang, G. D. Fuchs, D. A. Muller, and M. G. Spencer, Chemical vapor deposition growth of large single-crystal mono-, bi-, tri-layer hexagonal boron nitride and their interlayer stacking, ACS Nano **11**, 12057 (2017).

[18] M. Topsakal, E. Aktürk, and S. Ciraci, First-principles study of two- and one-dimensional honeycomb structures of boron nitride, Phys. Rev. B **79**, 115442 (2009).

[19] C. E. Ekuma, V. Dobrosavljević, and D. Gunlycke, First-Principles-Based Method for Electron Localization: Application to Monolayer Hexagonal Boron Nitride, Phys. Rev. Lett. **118**, 106404 (2017).

[20] R. M. Ribeiro and N. M. R. Peres, Stability of boron nitride bilayers: ground-state energies, interlayer distances, and tight-binding description, Phys. Rev. B **83**, 235312 (2011).

[21] D. Wickramaratne, L. Weston, and C. G. Van De Walle, Monolayer to bulk properties of hexagonal boron nitride, J. Phys. Chem. C **122**, 25524 (2018).

[22] T. C. Doan, J. Li, J. Y. Lin, and H. X. Jiang, Charge carrier transport properties in layer structured hexagonal boron nitride, AIP Adv. **4**, 107126 (2014).

[23] S. Bruzzone and G. Fiori, *Ab-initio* simulations of deformation potentials and electron mobility in chemically modified graphene and two-dimensional hexagonal boron-nitride, Appl. Phys. Lett. **99**, 222108 (2011).

[24] M. Bilal, W. Xu, C. Wang, H. Wen, X. Zhao, D. Song, and L. Ding, Optoelectronic properties of monolayer hexagonal boron nitride on different substrates measured by terahertz time-domain spectroscopy, Nanomaterials **10**, 762 (2020).

[25] W. G. Vandenberghe and M. V. Fischetti, Deformation potentials for band-to-band tunneling in silicon and germanium from first principles, Appl. Phys. Lett. **106**, 013505 (2015).

[26] T. Gunst, T. Markussen, K. Stokbro, and M. Brandbyge, First-principles method for electron-phonon coupling and electron mobility: applications to two-dimensional materials, Phys. Rev. B **93**, 035414 (2016).

[27] F. Giustino, Electron-phonon interactions from first principles, Rev. Mod. Phys. **89**, 015003 (2017).

[28] S. Poncé, E. R. Margine, and F. Giustino, Towards predictive many-body calculations of phonon-limited carrier mobilities in semiconductors, Phys. Rev. B **97**, 121201(R) (2018).

[29] L.-B. Shi, S. Cao, M. Yang, Q. You, K.-C. Zhang, Y. Bao, Y.-J. Zhang, Y.-Y. Niu, and P. Qian, Theoretical prediction of intrinsic electron mobility of monolayer InSe: first-principles calculation, J. Phys. Condens. Matter **32**, 065306 (2020).

[30] S. Poncé, W. Li, S. Reichardt, and F. Giustino, First-principles calculations of charge carrier mobility and conductivity in bulk semiconductors and two-dimensional materials, Rep. Prog. Phys. **83**, 036501 (2020).

[31] N. F. Hinsche and K. S. Thygesen, Electron-phonon interaction and transport properties of metallic bulk and monolayer transition metal dichalcogenide TaS_2, 2D Mater. **5**, 015009 (2017).

[32] T. Gunst, K. Kaasbjerg, and M. Brandbyge, Flexural-Phonon Scattering Induced by Electrostatic Gating in Graphene, Phys. Rev. Lett. **118**, 046601 (2017).

[33] P. B. Vyas, M. L. Van de Put, and M. V. Fischetti, Master-Equation Study of Quantum Transport in Realistic Semiconductor Devices Including Electron-Phonon and Surface-Roughness Scattering, Phys. Rev. Appl. **13**, 014067 (2020).

[34] G. Gaddemane, W. G. Vandenberghe, M. L. Van de Put, S. Chen, S. Tiwari, E. Chen, and M. V. Fischetti, Theoretical studies of electronic transport in monolayer and bilayer phosphorene: a critical overview, Phys. Rev. B **98**, 115416 (2018).

[35] M. M. Khatami, G. Gaddemane, M. L. Van de Put, M. V. Fischetti, M. K. Moravvej-Farshi, M. Pourfath, and W. G. Vandenberghe, First-principles study of the electron and hole mobility in silicane, in *2019 Device Research Conference (DRC)* (IEEE, Ann Arbor, 2019), pp. 127–128.

[36] G. Gaddemane, W. G. Vandenberghe, M. L. Van de Put, E. Chen, and M. V. Fischetti, Monte-Carlo study of electronic transport in non-σ_h-symmetric two-dimensional materials: silicene and germanene, J. Appl. Phys. **124**, 044306 (2018).

[37] N. D. Mermin and H. Wagner, Absence of Ferromagnetism or Antiferromagnetism in One- or Two-Dimensional Isotropic Heisenberg Models, Phys. Rev. Lett. **17**, 1133 (1966).

[38] P. C. Hohenberg, Existence of long-range order in one and two dimensions, Phys. Rev. **158**, 383 (1967).

[39] S. Coleman, There are no Goldstone bosons in two dimensions, Commun. Math. Phys. **31**, 259 (1973).

[40] M. V. Fischetti and W. G. Vandenberghe, Mermin-Wagner theorem, flexural modes, and degraded carrier mobility in two-dimensional crystals with broken horizontal mirror symmetry, Phys. Rev. B **93**, 155413 (2016).

[41] B. Amorim and F. Guinea, Flexural mode of graphene on a substrate, Phys. Rev. B **88**, 115418 (2013).

[42] Z.-Y. Ong and E. Pop, Effect of substrate modes on thermal transport in supported graphene, Phys. Rev. B **84**, 075471 (2011).

[43] O. D. Restrepo, K. E. Krymowski, J. Goldberger, and W. Windl, A first principles method to simulate electron mobilities in 2D materials, New J. Phys. **16**, 105009 (2014).

[44] T. Sohier, D. Campi, N. Marzari, and M. Gibertini, Mobility of two-dimensional materials from first principles in an accurate and automated framework, Phys. Rev. Mater. **2**, 114010 (2018).

[45] S. Takagi, A. Toriumi, M. Iwase, and H. Tango, On the universality of inversion layer mobility in Si MOSFET's: part II—effects of surface orientation, IEEE Trans. Electron Devices **41**, 2363 (1994).

[46] P. Giannozzi, S. Baroni, N. Bonini, M. Calandra, R. Car, C. Cavazzoni, D. Ceresoli, G. L. Chiarotti, M. Cococcioni, I. Dabo, A. Dal Corso, S. de Gironcoli, S. Fabris, G. Fratesi, R. Gebauer, U. Gerstmann, C. Gougoussis, A. Kokalj, M. Lazzeri, L. Martin-Samos *et al.*, QUANTUM ESPRESSO: a modular and open-source software project for quantum simulations of materials, J. Phys. Condens. Matter **21**, 395502 (2009).

[47] P. Giannozzi, O. Andreussi, T. Brumme, O. Bunau, M. Buongiorno Nardelli, M. Calandra, R. Car, C. Cavazzoni, D. Ceresoli, M. Cococcioni, N. Colonna, I. Carnimeo, A. Dal Corso, S. de Gironcoli, P. Delugas, R. A. DiStasio, A. Ferretti, A. Floris, G. Fratesi, G. Fugallo *et al.*, Advanced capabilities for materials modelling with QUANTUM ESPRESSO, J. Phys. Condens. Matter **29**, 465901 (2017).

[48] D. R. Hamann, Optimized norm-conserving Vanderbilt pseudopotentials, Phys. Rev. B **88**, 085117 (2013).

[49] J. P. Perdew, K. Burke, and M. Ernzerhof, Generalized Gradient Approximation Made Simple, Phys. Rev. Lett. **77**, 3865 (1996).

[50] H. J. Monkhorst and J. D. Pack, Special points for Brillouin-zone integrations, Phys. Rev. B **13**, 5188 (1976).

[51] T. Sohier, M. Calandra, and F. Mauri, Density functional perturbation theory for gated two-dimensional heterostructures: theoretical developments and application to flexural phonons in graphene, Phys. Rev. B **96**, 075448 (2017).

[52] N. Marzari and D. Vanderbilt, Maximally localized generalized Wannier functions for composite energy bands, Phys. Rev. B **56**, 12847 (1997).

[53] F. Giustino, M. L. Cohen, and S. G. Louie, Electron-phonon interaction using Wannier functions, Phys. Rev. B **76**, 165108 (2007).

[54] S. Poncé, E. R. Margine, C. Verdi, and F. Giustino, EPW: electron-phonon coupling, transport and superconducting

properties using maximally localized Wannier functions, Comput. Phys. Commun. **209**, 116 (2016).

[55] C. Jacoboni and L. Reggiani, The Monte Carlo method for the solution of charge transport in semiconductors with applications to covalent materials, Rev. Mod. Phys. **55**, 645 (1983).

[56] F. Ferreira, A. J. Chaves, N. M. R. Peres, and R. M. Ribeiro, Excitons in hexagonal boron nitride single-layer: a new platform for polaritonics in the ultraviolet, J. Opt. Soc. Am. B **36**, 674 (2019).

[57] M. M. Khatami, G. Gaddemane, M. L. Van De Put, M. K. Moravvej-Farshi, and W. G. Vandenberghe, Electronic transport properties of hydrogenated and fluorinated graphene: a computational study, J. Phys. Condens. Matter **32**, 495502 (2020).

[58] A. Burk, M. O'Loughlin, R. Siergiej, A. Agarwal, S. Sriram, R. Clarke, M. MacMillan, V. Balakrishna, and C. Brandt, SiC and GaN wide bandgap semiconductor materials and devices, Solid. State. Electron. **43**, 1459 (1999).

[59] C. J. H. Wort and R. S. Balmer, Diamond as an electronic material, Mater. Today **11**, 22 (2008).

[60] See Supplemental Material at http://link.aps.org/supplemental/10.1103/PhysRevB.104.235424 for the electron-phonon interaction matrix elements in germanane and hexagonal boron nitride as depicted in Figs. S1–S4.

[61] C. Verdi and F. Giustino, Fröhlich Electron-Phonon Vertex from First Principles, Phys. Rev. Lett. **115**, 176401 (2015).

[62] L. Cheng and Y. Liu, What limits the intrinsic mobility of electrons and holes in two dimensional metal dichalcogenides? J. Am. Chem. Soc. **140**, 17895 (2018).

[63] X. Li, J. T. Mullen, Z. Jin, K. M. Borysenko, M. Buongiorno Nardelli, and K. W. Kim, Intrinsic electrical transport properties of monolayer silicene and MoS_2 from first principles, Phys. Rev. B **87**, 115418 (2013).

[64] K. Kaasbjerg, K. S. Thygesen, and K. W. Jacobsen, Phonon-limited mobility in *n*-type single-layer MoS_2 from first principles, Phys. Rev. B **85**, 115317 (2012).

[65] T. Sohier, M. Calandra, and F. Mauri, Two-dimensional Fröhlich interaction in transition-metal dichalcogenide monolayers: theoretical modeling and first-principles calculations, Phys. Rev. B **94**, 085415 (2016).

[66] M. M. Khatami, G. Gaddemane, M. L. Van de Put, M. V. Fischetti, M. K. Moravvej-Farshi, M. Pourfath, and W. G. Vandenberghe, Electronic transport properties of silicane determined from first principles, Materials **12**, 2935 (2019).

[67] J. B. Gunn and B. J. Elliott, Measurement of the negative differential mobility of electron in GaAs, Phys. Lett. **22**, 369 (1966).

[68] P. N. Butcher, The Gunn effect, Rep. Prog. Phys. **30**, 303 (1967).

[69] J. Fang, M. V. Fischetti, R. D. Schrimpf, R. A. Reed, E. Bellotti, and S. T. Pantelides, Electron Transport Properties of $Al_xGa_{1-x}N$/GaN Transistors Based on First-Principles Calculations and Boltzmann-Equation Monte Carlo Simulations, Phys. Rev. Appl. **11**, 044045 (2019).

[70] L. Cheng, C. Zhang, and Y. Liu, Why Two-Dimensional Semiconductors Generally Have Low Electron Mobility, Phys. Rev. Lett. **125**, 177701 (2020).

[71] L. Cheng, C. Zhang, and Y. Liu, Intrinsic charge carrier mobility of 2D semiconductors, Comput. Mater. Sci. **194**, 110468 (2021).

[72] S. Gopalan, G. Gaddemane, M. L. Van de Put, and M. V. Fischetti, Monte Carlo study of electronic transport in monolayer InSe, Materials **12**, 4210 (2019).

[73] Z. Jin, X. Li, J. T. Mullen, and K. W. Kim, Intrinsic transport properties of electrons and holes in monolayer transition-metal dichalcogenides, Phys. Rev. B **90**, 045422 (2014).

[74] C. Jacoboni, C. Canali, G. Ottaviani, and A. Alberigi Quaranta, A review of some charge transport properties of silicon, Solid State Electron. **20**, 77 (1977).

[75] Z. Aksamija, H.-S. Hahm, and U. Ravaioli, Emission and absorption of phonons in silicon, Phys. Status Solidi Curr. Top. Solid State Phys. **5**, 90 (2008).